International Journal of Engineering & Technology
CENTRE OF PROFESSIONAL RESEARCH PUBLICATIONS
ISSN 2049-3444
International Journal of Engineering and Technology Volume 6 No.8, August, 2016

Dynamics of a Four Quadrant Chopper Controlled D.C Machine at a Regulated Duty Cycle and Machine Speed for Efficient Drive Performance

C. O. Omeje
Department of Electrical Engineering, University of Port Harcourt, Rivers State, Nigeria

ABSTRACT

Direct current (d.c) motors umpteen times are used in most adjustable speed drives and position controlled applications. They usually draw a very high armature current during starting which is usually higher than its rated value due to negligible back emf. This current value is often lethal to the commutator which conventionally should not have a current value greater than twice the rated value. To curb this hazardous effect of excess armature current, the d.c motor with separately excited d.c machine operation is regulated through a d.c armature voltage supply using a four quadrant duty cycle controlled chopper with variable d.c voltage output. This paper therefore explored the significances of attenuating the dangerous effect of high starting current on the commutator of the d.c machine using the voltage control method derived from duty cycle adjustment. Optimal drive performances with three different controlled closed loops were analyzed and achieved through simulation in MATLAB 7.11 to test for the machine speed responses and peak armature current values at duty cycles of 0.4, 0.6 and 0.8 respectively. Speed regulation values of -0.0018rad/Nm, -0.0491rad/Nm and -0.1159rad/Nm were obtained for the three closed loops. The control analysis showed that closed loop with a PI-controller gave the least transient and best steady state characteristics.

Key words: *Four Quadrant Chopper, Separately Excited D.C Motors, Control Loops, Speed-Torque Control, P.I Controllers, Dynamic Modeling, MATLAB Simulations.*

1. INTRODUCTION

Electric motor drives have formed essential parts of most industrial applications. In modern electric drive system, power electronic converters are extensively used for adjustable frequency and voltage control [1]. DC drives are widely used in applications requiring adjustable speed control such as traction application, paper mills, rolling mills, mine winder, hoist and printing press [2]. The speed of DC motors can be adjusted above or below rated speed. The speed above rated speed is controlled by field flux whilst below rated speed is by armature voltage control method [3]. In reference [4], speed control of dc motor using four quadrant chopper was considered without a detailed simulation analysis on feedback and embedded P-I controller. In [5], four quadrant operation of chopper fed separately excited dc motor was analyzed in terms of decoupled PWM control using digital signal processor (DSP) but had limitations in determining the rate of speed response to transient and steady state error using P-I controller. Similar work done in [6] discussed and modeled separately excited dc motor speed control using four quadrant chopper under a varying speed and load torque conditions with no reference to peak armature current control achieved through the four quadrant duty cycle adjustment. The performance characteristics of a controlled separately excited dc motor was considered in [7] with emphasis on the transient behaviour of various dc machines without detailed consideration on the armature current, speed and torque control of the machine with a well modeled four quadrant chopper at a regulated duty cycle. In this paper, speed control and peak armature current value was achieved through a well adjusted duty cycle of 40%, 60% and 80% values from a four quadrant dc chopper. This in turn attenuated the effect of undue harmonics inherent in the starting current of the machine. The dynamic performance of a separately excited dc motor with constant field excitation was investigated while a three closed loop control schemes were analyzed in terms of speed response to transient and steady state condition. The first closed loop has an embedded speed controller. The second closed loop has both speed controller and inner current gain. The third closed loop has speed controller, inner current gain and P-I controller. In these closed loops control, the externally applied controller and feedback gains were adjusted to give excellent drive performance in terms of quicker steady state response time and good speed regulation.

2. BASIC OPERATION OF A FOUR QUADRANT CHOPPER

DC Choppers provide smooth acceleration control, high efficiency and fast dynamic response. They are widely used in traction applications and in most electric automobiles such as trolley cars, marine hoists, fork-lift trucks and mine haulers [8, 9]. Choppers can be used in regenerative braking of dc motors to return energy to the supply and this feature according to Rashid [10], results in energy savings for transportation system with frequent stopping. Choppers are used in dc voltage regulators and in conjunction with an inductor to generate a dc current source inverter [11]. The circuit diagram shown in figure 1 depicts the four quadrant dc chopper circuit.

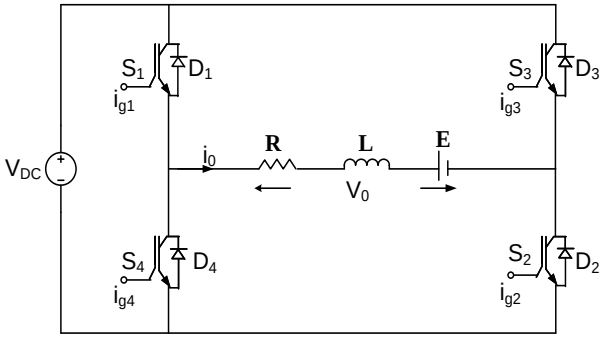

Figure 1: Four Quadrant d.c Chopper Circuit

The basic operation of figure 1 is to switch on the positive axis of the d.c source voltage across the load for the first half cycle and then switch on the negative axis of the d.c source voltage across the load for the remaining half cycle [12, 13]. The converter under this condition operates only in the continuous load current mode as discussed in [14].

At an interval of $0 \leq t \leq DT$, **S_1** and **S_2** are turned on. The load current flows through the loop comprising **V_{DC}, S_1D_1, RLE** and **S_2 D_2** thus impressing a load voltage magnitude that is equal to the positive supply voltage. During this operational mode, the differential equation in accordance with Kirchhoff's rule is represented by (1) for $0 \leq t \leq T_{on}$.

$$V_0 = V_S = Ri_0 + L\frac{di_0}{dt} + E \qquad (1)$$

At an interval of $T_{on} < t \leq T$, S_1 is turned off while the load current continues to flow through the freewheeling diode. The differential equation in (1) under this condition transforms into (2).

$$0 = V_S = Ri_0 + L\frac{di_0}{dt} + E \qquad (2)$$

Taking a Laplace transformation of (1) and (2) gives rise to (3) and (4) in frequency domain.

$$\frac{V_s - E}{S} = RI_{(s)} + L[SI_{(s)} - I_{01}] \qquad (3)$$

$$-\frac{E}{S} = RI_{(s)} + L[SI_{(s)} - I_{02}] \qquad (4)$$

Re-arranging (3) and (4) in terms of current equation gives rise to (5) and (6).

$$I_{(s)} = \frac{V_s - E}{S(R+SL)} + \frac{L.I_{01}}{R+SL} = \frac{V_s - E}{SL\left(S+\frac{R}{L}\right)} + \frac{I_{01}}{S+\frac{R}{L}} \qquad (5)$$

$$I_{(s)} = \frac{-E}{S(R+SL)} + \frac{L.I_{02}}{R+SL} = \frac{-E}{SL\left(S+\frac{R}{L}\right)} + \frac{I_{02}}{S+\frac{R}{L}} \qquad (6)$$

Taking a Laplace inverse transform of (5) gives rise to (7) in time domain for $0 < t \leq T_{on}$.

$$i_{(t)} = \frac{V_s - E}{S}\left(1 - e^{-\frac{R}{L}t}\right) + I_{01}e^{-\frac{R}{L}t} \qquad (7)$$

Similarly, time domain current expression in (6) for $T_{on} < t \leq T$ is given by (8).

$$i_{(t^1)} = -\frac{E}{R}\left(1 - e^{-\frac{R}{L}t^1}\right) + I_{02}e^{-\frac{R}{L}t^1} \qquad (8)$$

Where $t^1 = t - T_{on}$

At a time interval of $DT \leq t \leq T$, **S_3** and **S_4** are turned on with **S_1** and **S_3** simultaneously turned off. The load current thus flows in the loop comprising **V_{DC}, S_3D_3, RLE** and **S_4D_4**.

When $t = T_{on}$, $i_{(t)} = I_{02}$ which gives rise to (9).

$$I_{02} = \frac{V_s - E}{R}\left(1 - e^{-\frac{T_{on}}{\tau}}\right) + I_{01}e^{-\frac{T_{on}}{\tau}} \qquad (9)$$

At $t^1 = T_{off} = T - T_{on}$, $i_{(t^1)} = I_{01}$ giving rise to (10).

$$I_{01} = -\frac{E}{R}\left(1 - e^{-\frac{(T-T_{on})}{\tau}}\right) + I_{01}e^{-\frac{(T-T_{on})}{\tau}} \qquad (10)$$

Simultaneous solution of (9) and (10) gives rise to (11) and (12).

$$I_{01} = \frac{V_s}{R}\left[\frac{1 - 2e^{\frac{DT}{\tau}} + e^{\frac{T}{\tau}}}{1 - e^{\frac{T}{\tau}}}\right] - \frac{E}{R} \qquad (11)$$

$$I_{02} = \frac{V_s}{R}\left[\frac{1 - 2e^{-\frac{DT}{\tau}} + e^{-\frac{T}{\tau}}}{1 - e^{-\frac{T}{\tau}}}\right] - \frac{E}{R} \qquad (12)$$

The swing in the choppers load current is represented by (13)

$$I_{02} - I_{01} = \frac{2V_s}{R}\left[\frac{1 - e^{-\frac{DT}{\tau}} - e^{-\frac{(1-D)T}{\tau}} + e^{-\frac{T}{\tau}}}{1 - e^{-\frac{T}{\tau}}}\right] \qquad (13)$$

The maximum value of this swing occurs at a duty cycle of D = 0.5 as given in (14)

$$(I_{02} - I_{01})_{max} = \frac{2V_s}{R}\left[\frac{1 - e^{-\frac{T}{2\tau}}}{1 - e^{-\frac{T}{2\tau}}}\right] \qquad (14)$$

The switching sequence of the four quadrant chopper is presented in figure 2.

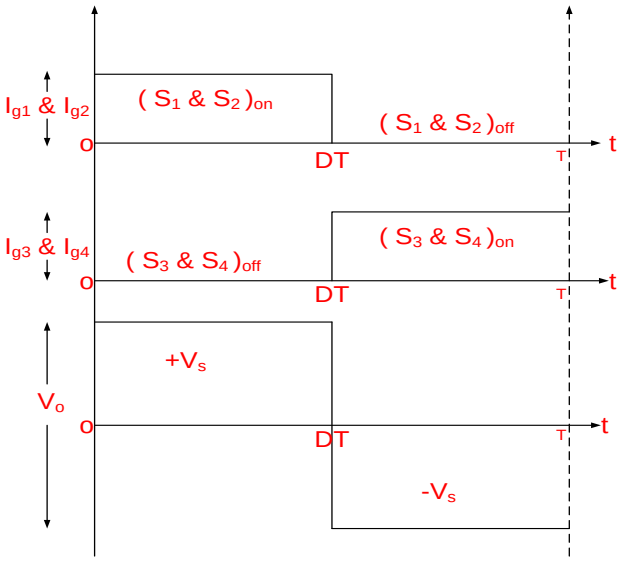

Figure 2: Switching Sequence of a four quadrant Chopper

The average output voltage is readily computed from figure 2 by taking an integral over the square waveform as represented in (15).

$$V_0 = \frac{1}{T}\int_0^T V_0 dt = \frac{1}{T}\left[\int_0^{DT} V_S dt - \int_{DT}^{T} V_S dt\right]$$
$$= V_S(2D-1) \qquad (15)$$

The average load output voltage in (15) thus varies from the positive value of the supply voltage to the negative value as the duty cycle (D) varies from zero through 0.5 to unity. This variation in the duty cycles regulates the magnitude of the output voltage of the chopper that is fed to the dc machine which in turn controls the rate of armature current rise during starting operation and also regulates the motor speed.

3.1. DC Motor Steady State Speed and Torque Control

The equivalent circuit of a separately excited d.c machine is shown in figure 3.

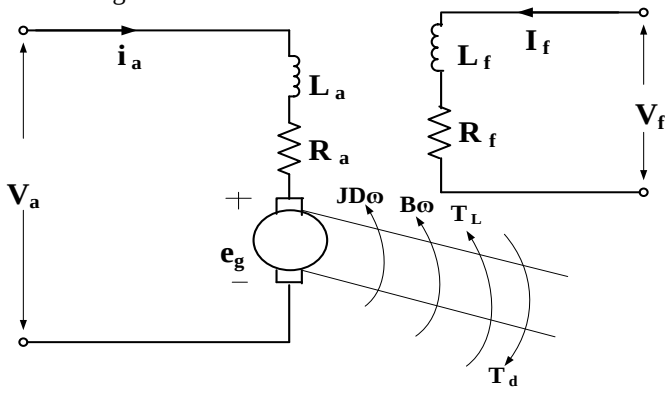

Figure 3: Equivalent Circuit of separately excited d.c machine

The basic equations of a dc machine derived from figure 3 are presented in (16)-(19).

$$e_g = K\phi\omega_m \qquad (16)$$

$$V_a = R_a i_a + L_a\frac{di_a}{dt} + e_g \qquad (17)$$

$$T = K\phi i_a \qquad (18)$$

$$V_f = R_f i_f + L_f\frac{di_f}{dt} \qquad (19)$$

At a steady state condition of the machine, $\frac{di_a}{dt} = \frac{di_f}{dt} = 0$. Thus, the armature voltage equation changes to (20) with motor speed represented in (21) and (22) in terms of armature current and torque.

$$V_a = R_a i_a + e_g \qquad (20)$$

$$\omega_m = \frac{V_a}{K\phi} - \frac{R_a}{K\phi} i_a \qquad (21)$$

$$\omega_m = \frac{V_a}{K\phi} - \frac{R_a}{(K\phi)^2} T \qquad (22)$$

Where ω = motor speed in rad/second.

K_ϕ = Field excitation constant in Volt/Amp-rad/sec.

L_a = Armature circuit inductance in Henry,

L_f = Field circuit inductance in Henry,

R_a = Armature Circuit Resistance in Ω,

R_f= Field Circuit Resistance in Ω, T = Torque Developed in Nm.

i_a= Armature current in A, i_f = Field current in A

The above three principal equations are essential in the steady state analysis of a dc motor speed and torque control characteristics [15]. In practical terms, if the armature voltage of a separately excited dc motor running at a steady state condition decreases by a small magnitude, the armature current and the motor torque decrease proportionately. When this decrease in armature voltage persists in greater magnitude, the motor decelerates to a point where the value of the armature voltage becomes less than the back emf. At this point, the armature current is forced to reverse in direction with the dc motor producing a negative torque which under this condition functions as a generator. Conversely, if the armature voltage of a d.c motor running at a steady state speed is increased, the armature current and the motor torque increase with a resultant motor acceleration. This increase in speed invariably causes a step increase in the back emf. A large increase in armature voltage causes a large inflow of armature current which may destroy the commutator. To curb this effect, the variable dc voltage is regulated with a controlled rectifier or a dc chopper. Similarly, when the field of a separately excited dc motor running at a rated speed is weakened, it's induced emf decreases in the field flux as a result the torque is increased by a large amount which considerably is greater than the load torque. This causes the motor to accelerate with a corresponding rise in the load torque. Thus, further

weakening of the field by a large amount will cause a dangerous inrush of current. In like manner, increasing the field of the machine increases the back emf which may exceed the armature voltage. At this condition, the armature current reduces and often reverses in direction. This propels the machine to work as a generator thereby feeding energy to the supply system. The MATLAB plots in figures 4-7 represent the variations in speed and torque with respect to changes in values of the armature voltage, field excitation and armature circuit resistance at different operating conditions.

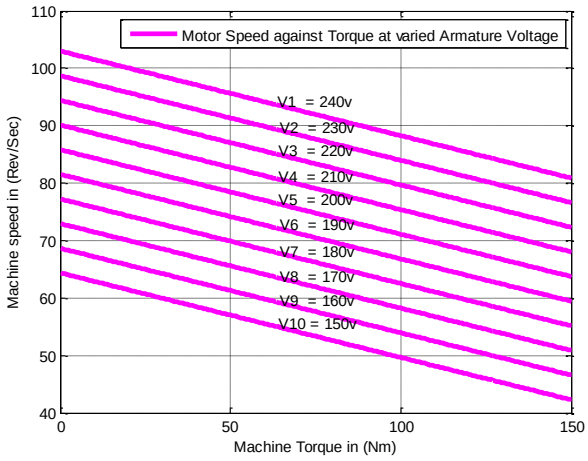

Figure 4 Speed-Torque at varied Armature Voltage

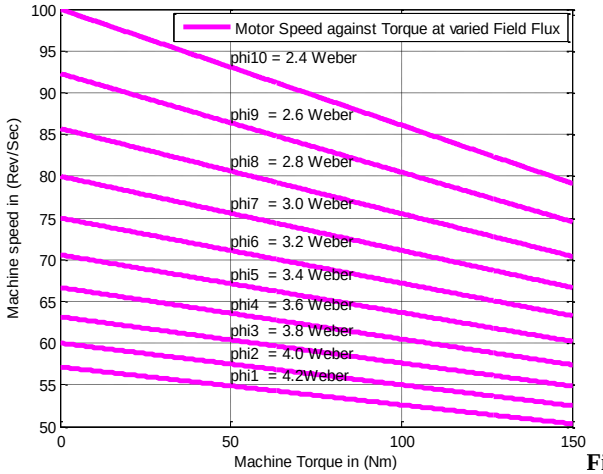

Figure 5 Speed-Torque at varied Field Flux

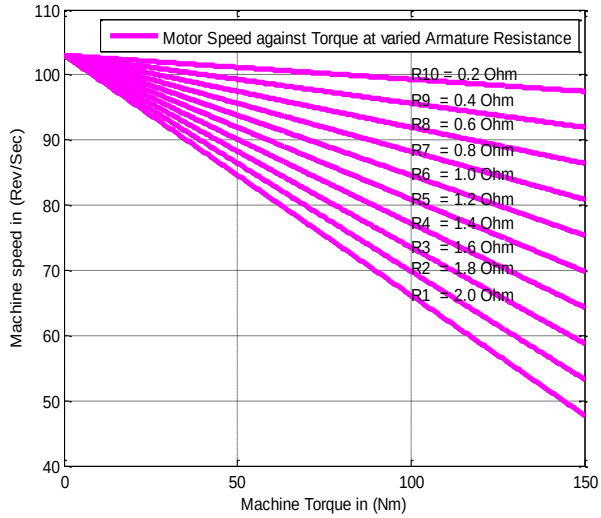

Figure6 Speed-Torque at varied Resistance

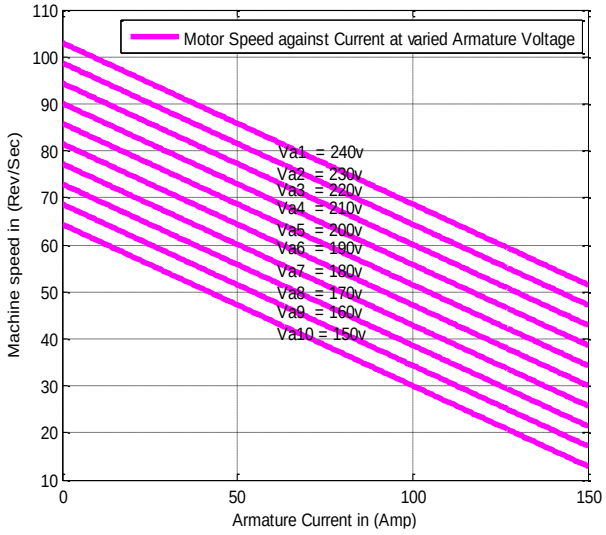

Figure7 Speed-Current at varied Armature Voltage

3.2. Dynamic Modeling of Closed Loop Control System of a Separately Excited dc Machine

The dynamic model of the closed loop was derived from the basic equations of a separately excited dc motor already shown in (16) – (19) with a slight modification in the motor developed torque as presented in (23).

$$T_d = K\phi i_a = J\frac{d\omega}{dt} + \beta\omega + T_L \qquad (23)$$

Transforming (17), (19) and (23) into frequency domain produces (24)-(29).

$$V_{a(s)} = R_a I_{a(s)} + SL_a I_{a(s)} + K_\phi \omega_{(s)} \qquad (24)$$

$$I_{a(s)} = \frac{V_{a(s)} - K_\phi \omega_{(s)}}{SL_a + R_a} \qquad (25)$$

$$V_{f(s)} = R_f I_{f(s)} + SL_f I_{f(s)} \quad (26)$$

$$I_{f(s)} = \frac{V_{f(s)}}{SL_f + R_f} \quad (27)$$

$$T_{d(s)} = K_\phi I_{a(s)} + SJ\omega_{(s)} + \beta\omega_{(s)} + T_{L(s)} \quad (28)$$

$$\omega_{(s)} = \frac{T_{d(s)} - T_{L(s)}}{SJ + \beta} \quad (29)$$

The scope of this modeling concentrated on three different closed loop controlled schemes which are classified in terms of their feedback controlled parameters as illustrated in figures 8, 9 & 10. The closed loop controlled system block of the separately excited dc machine with speed controller and tachometer feedback is presented in figure 8.

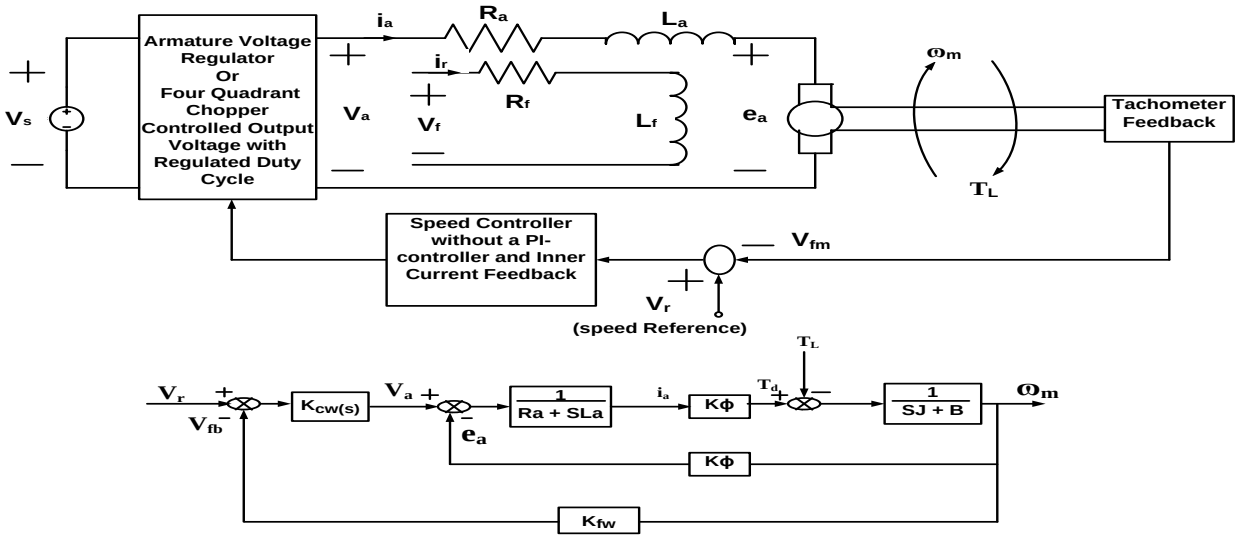

Figure 8 Closed loop control block with speed controller

The dynamic equation for the control block diagram of figure 8 in terms of the transfer function is represented in (30).

$$\begin{pmatrix} \omega_{m(s)} \\ i_{a(s)} \end{pmatrix} = \begin{pmatrix} \frac{G_{11}}{D_{w(s)}} & \frac{G_{12}}{D_{w(s)}} \\ \frac{G_{21}}{D_{w(s)}} & \frac{G_{22}}{D_{w(s)}} \end{pmatrix} \begin{pmatrix} V_{r(s)} \\ T_{L(s)} \end{pmatrix} \quad (30)$$

$G_{11} = K_\phi K_{cw(s)}$, $G_{12} = -(R_a + SL_a)$,

$G_{21} = (SJ + B)K_{cw(s)}$ and

$G_{22} = K_\phi + K_{fw}K_{cw(s)}$

Where $D_{w(s)} = S^2 JL_a + S(R_a J + BL_a) + R_a B + (K_\phi)^2 + K_\phi K_{fw} K_{cw(s)}$ (31)

The characteristic polynomial equation in second order is derived by re-writing (31) to (32)

$$D_{w(s)} = S^2 + \frac{(R_a J + BL_a)S}{JL_a} + \frac{(K_\phi)^2 + R_a B + K_\phi K_{fw} K_{cw(s)}}{JL_a} \quad (32)$$

The conventional second order control equation is represented by (33)

$$S^2 + 2S\varepsilon_n\omega_n + (\omega_n)^2 = 0 \quad (33)$$

Comparing (32) and (33) gives rise to (34) and (35).

$$\omega_n = \sqrt{\frac{(K_\phi)^2 + R_a B + K_\phi K_{fw} K_{cw(s)}}{JL_a}} \quad (34)$$

$$\varepsilon_n = \frac{(R_a J + BL_a)}{2JL_a\omega_n} \quad (35)$$

The natural frequency is represented by (34) while (35) represents the damping ratio.

The steady state speed per unit torque or speed regulation (SR) is given by (36).

$$\frac{\Delta\omega_{m(S=0)}}{\Delta T_{L(S=0)}} = SR = \frac{-R_a}{(K_\phi)^2 + R_a B + K_\phi K_{fw} K_{cw(s)}} \quad (36)$$

An enhanced closed loop controlled system with the inner current gain which improves the speed response of the machine is presented in figure 9 while the dynamic equation for the control

block diagram in terms of the transfer function is represented in (37).

$$\begin{pmatrix} \omega_{m(s)} \\ i_{a(s)} \end{pmatrix} = \begin{pmatrix} \frac{G_{11}}{D_{w(s)}} & \frac{G_{12}}{D_{w(s)}} \\ \frac{G_{21}}{D_{w(s)}} & \frac{G_{22}}{D_{w(s)}} \end{pmatrix} \begin{pmatrix} V_{r(s)} \\ T_{L(s)} \end{pmatrix} \quad (37)$$

$G_{11} = K_{\phi} K_{cw(s)} K_{ci(s)}$,

$G_{12} = -(R_a + SL_a + K_{fi} K_{ci})$,

$G_{21} = (SJ + B) K_{cw(s)} K_{ci(s)}$,

$G_{22} = K_{\phi} + K_{cw(s)} K_{ci(s)} K_{fw}$.

Where: $D_{w(s)} = S^2 JL_a + S(R_a J + BL_a + JK_{fi(s)} K_{ci(s)}) + R_a B + K_{\phi} K_{cw(s)} K_{ci(s)} K_{fw} + (K_{\phi})^2 + BK_{ci(s)} K_{fi(s)}$ (38)

The characteristic second order polynomial equation is derived by re-writing (38) to (39)

$$D_{w(s)} = S^2 + \frac{A_{11}}{JL_a} + \frac{A_{12}}{JL_a} \quad (39)$$

Where: $A_{11} = S(R_a J + BL_a + JK_{fi(s)} K_{ci(s)})$ and

$A_{12} = R_a B + K_{\phi} K_{cw(s)} K_{ci(s)} K_{fw} + (K_{\phi})^2 + BK_{ci(s)} K_{fi(s)}$

Comparing (39) with (33) gives rise to (40) and (41).

$$\omega_n = \sqrt{\frac{X}{JL_a}} \quad (40)$$

Where: $X = R_a B + K_{\phi} K_{cw(s)} K_{ci(s)} K_{fw} + (K_{\phi})^2 + BK_{ci(s)} K_{fi(s)}$

$$\varepsilon_n = \frac{(R_a J + BL_a + JK_{fi(s)} K_{ci(s)})}{2 \times JL_a \omega_n} \quad (41)$$

The natural frequency is represented by (40) while (41) represents the damping ratio.

The steady state speed per unit torque or speed regulation (SR) is given by (42).

$$\frac{\Delta \omega_{m(S=0)}}{\Delta T_{L(S=0)}} = \frac{-(R_a + K_{fi} K_{ci})}{Q_1} \quad (42)$$

Where: $Q_1 = R_a B + K_{\phi} K_{cw(s)} K_{ci(s)} K_{fw} + (K_{\phi})^2 + BK_{ci(s)} K_{fi(s)}$

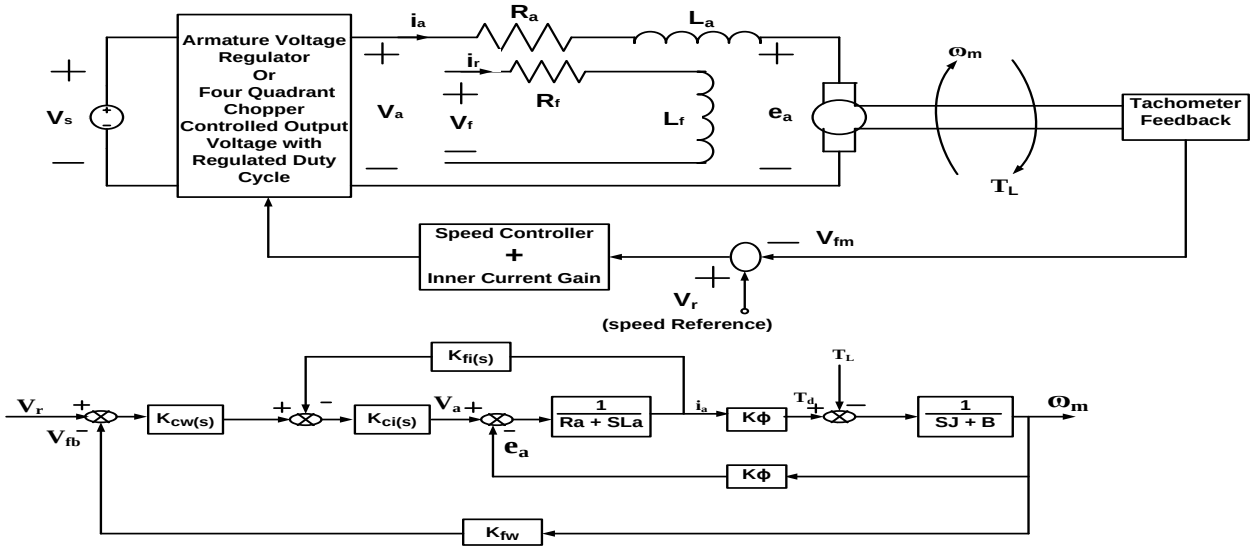

Figure 9 Closed loop control block with speed controller + Inner Current Gain

Generally, speed control with inner current loop considerably reduces the transient level in the system response time to input step change in motor speed, armature current and torque. Therefore, with the incorporation of a PI-controller as presented in figure 10, the steady state speed error is reduced with an appreciable low transient peak armature current value as shown in the simulation results. A much reduced damping and better speed regulation value is also associated with this control method.

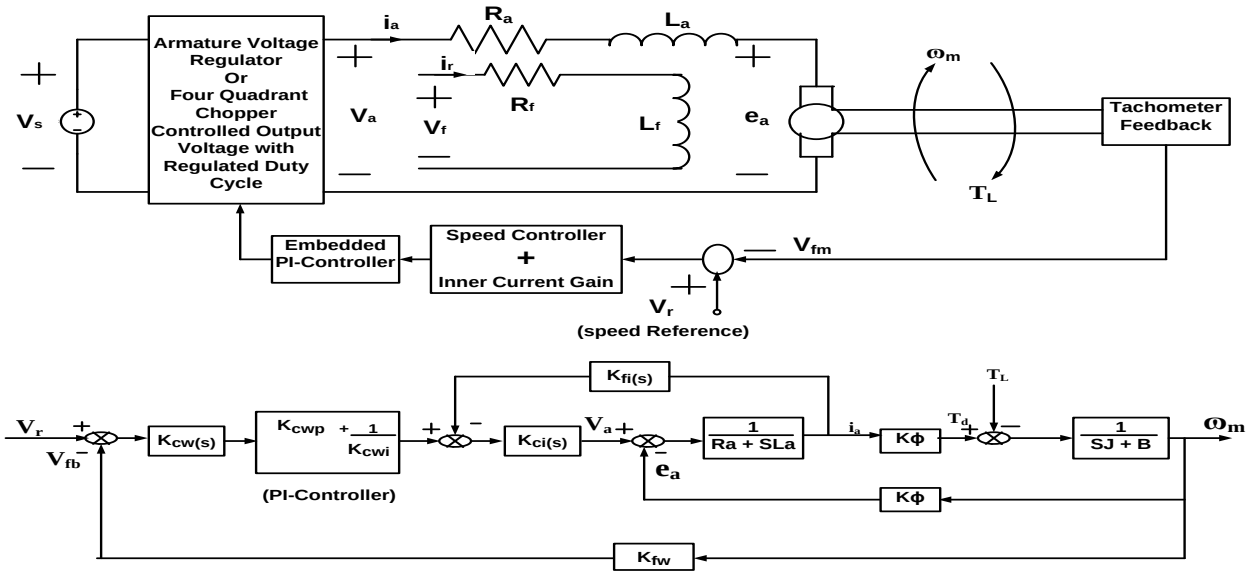

Figure 10 Closed loop control block with speed controller + Inner Current Gain + PI-Controller

The dynamic equation of figure 10 is presented in (43) while the steady state speed rise per unit increase in torque also called speed regulation (SR) is represented by (45).

$$\begin{pmatrix}\omega_{m(s)}\\ i_{a(s)}\end{pmatrix} = \begin{pmatrix}\frac{G_{11}}{D_{w(s)}} & \frac{G_{12}}{D_{w(s)}}\\ \frac{G_{21}}{D_{w(s)}} & \frac{G_{22}}{D_{w(s)}}\end{pmatrix}\begin{pmatrix}V_{r(s)}\\ T_{L(s)}\end{pmatrix} \qquad (43)$$

Where: $G_{11} = K_\phi K_{cw(s)} K_{ci(s)} \left(K_{cwp} + \frac{K_{cwi}}{S}\right)$,

$G_{12} = -(R_a + SL_a + K_{fi}K_{ci})$,

$G_{21} = (SJ + B)K_{cw(s)}K_{ci(s)}\left(K_{cwp} + \frac{K_{cwi}}{S}\right)$ and

$G_{22} = K_\phi + K_{cw(s)}K_{ci(s)}K_{fw(s)}\left(K_{cwp} + \frac{K_{cwi}}{S}\right)$

$$D_{w(s)} = S^2JL_a + S(R_aJ + BL_a + JK_{ci}K_{fi}) + \frac{K_{cw(s)}K_{ci(s)}K_\phi K_{fw(s)}K_{cwi}}{S} + R_aB + K_\phi K_{cw(s)}K_{ci(s)}K_{fw(s)}K_{cwp} + (K_\phi)^2 + BK_{ci(s)}K_{fi(s)} \qquad (44)$$

$$\frac{\Delta\omega_{m(S=0)}}{\Delta T_{L(S=0)}} = (SR) = \frac{-(R_a + K_{fi}K_{ci})}{Q_2} \qquad (45)$$

Where: $Q_2 = R_aB + K_\phi K_{cw(s)}K_{ci(s)}K_{fw(s)}K_{cwp} + (K_\phi)^2 + BK_{ci(s)}K_{fi(s)}$

The characteristic polynomial equation in (44) when properly resolved is a third order equation and thus cannot be compared in terms of the damping factor though simulation results showed a high reduction in the value of damping as the machine is set into motion.

4. SIMULATION RESULTS AND DISCUSSION

Simulations of the three closed loop controlled schemes for the separately excited dc machine were carried out in Matlab/Simulink environment with the motor parameters presented in table 1. The simulation was done at three different regulated duty cycles to test for the efficiency level of the machine running performance in terms of peak armature current, running speed, motor torque, expected output power and corresponding speed regulation values. The results presented in figures 11-13 represent the controls signals for the four quadrant chopper at a regulated duty cycles of 0.8, 0.6 and 0.4 respectively. In figure 14, a high starting armature current, motor developed torque and speed were produced for the closed loop with speed controller at 0.8 duty cycle. This high current value when not properly handled could be dangerous to the commutator. In figure 15, a reduction in the values of armature current and developed torque with a corresponding decrease in the speed of the machine was observed for a closed loop with speed controller and inner current gain at 0.8 duty cycle. This reduction in high armature current value reduces the undue shaft and heat losses associated with high armature current in figure 14. In figure 16, an appreciable decrease in the value of armature current, developed torque and motor speed were obtained with a closed loop having a speed controller and inner current gain with an embedded PI-controller at 0.8 duty cycle. It is obvious that the transience state was reduced and a better steady state operation was achieved with this closed loop control scheme thus allowing for efficient drive performance. In figures 17-19, it is evidently shown that at a regulated duty cycle of 0.6, an obvious decrease in the chopper output voltage fed to the separately excited d.c machine was produced which is in accordance with equation (15). This decrease in voltage magnitude is also affected by the peak value of the armature transient current, developed torque and motor speed. This voltage control method is industrially

applied in armature current control. In figures 20-22, a common but significant characteristic was observed at 0.4 duty cycle. The d.c machine runs at a negative speed value and produces a positive value of motor developed torque. This is indicative of reverse braking characteristics of the machine since energy is being pumped back to the source of supply.

Table 1: Simulation Parameters

Variable	Values
Four quadrant Chopper Variable dc output voltage V_0	220V
Armature Resistance R_a (Ω)	0.0130
Armature Inductance L_a (H)	0.010
Machine moment of Inertia J (Kgm^2)	0.201
Coefficient of Viscous Friction B (Nm^2)	0.0001074
Load Torque T_L (Nm)	55
Field excitation constant $K\phi$	1.337
Tachometer gain K_{fw}	0.04244
Inner current gain Kci(s)	1.112
Inner current feedback K_{Fi}	0.333
Speed controller gain $K_{cw(s)}$	96.4
Chopper switching frequency F_s (Hz)	4000
Chopper duty cycles	0.4, 0.6 & 0.8
PI-controller gain	$0.25\left(1+\frac{0.01}{S}\right)$

Table 2: Closed Loops Speed Regulation Values

Closed Loop Type	Speed Regulation (SR) Value
Closed Loop with Speed Controller only	-0.0018rad/Nm
Closed Loop with Speed Controller + Inner Current Gain	-0.0491rad/Nm
Closed Loop with Speed Controller + Inner Current Gain + PI-Controller	-0.1159rad/Nm

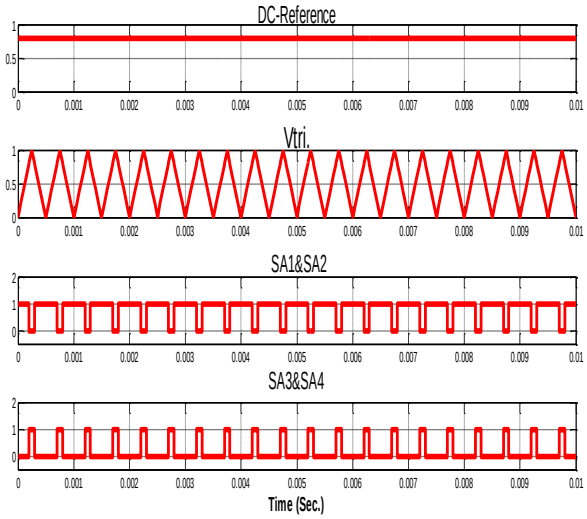

Figure 11 Firing signals at 0.8 duty cycle.

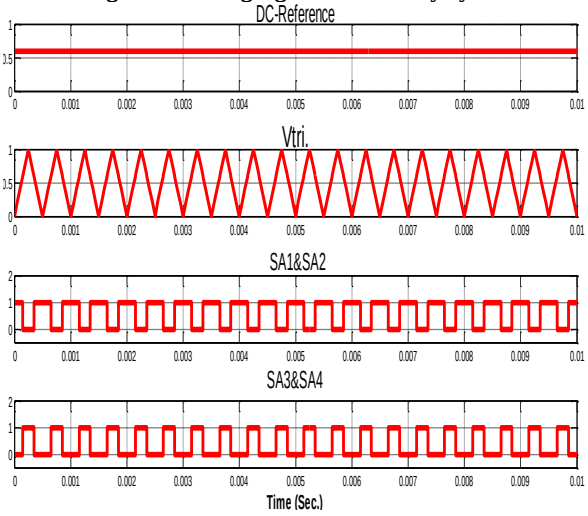

Figure 12 Firing signals at 0.6 duty cycle.

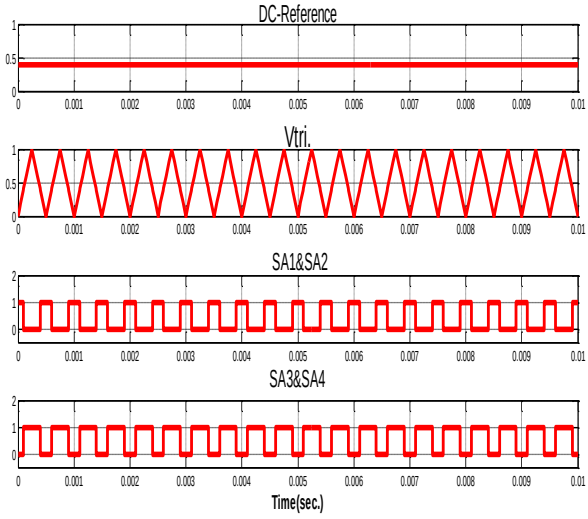

Figure 13 Firing signals at 0.4 duty cycle.

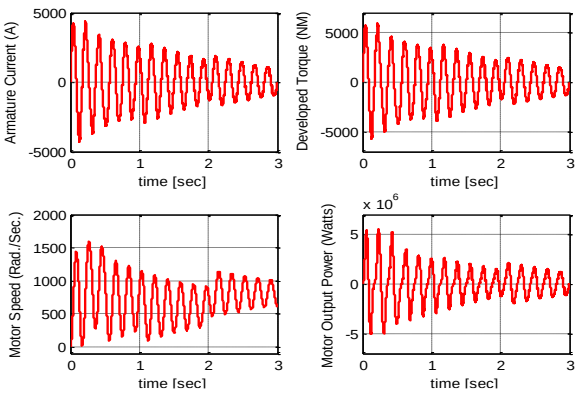

Figure 14 Closed loop characteristics with speed controller at 0.8 duty cycle.

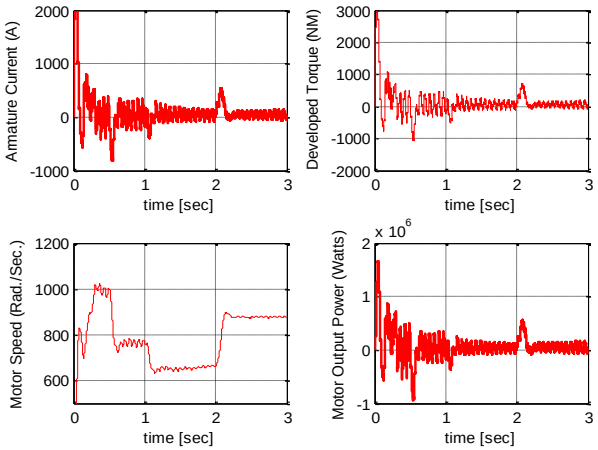

Figure 15 Closed loop characteristics with speed controller + Inner current gain at 0.8 duty cycle.

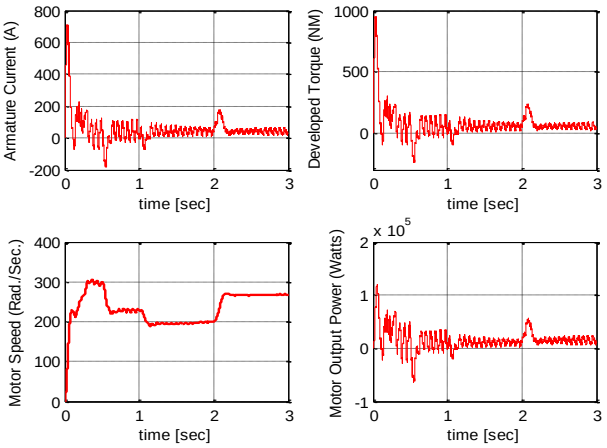

Figure 16 Closed loop characteristics with speed controller + Inner current gain + PI-Controller at 0.8 duty cycle.

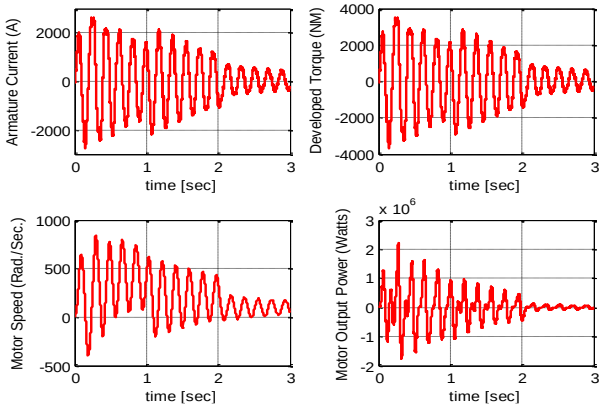

Figure 17 Closed loop characteristics with speed controller at 0.6 duty cycle.

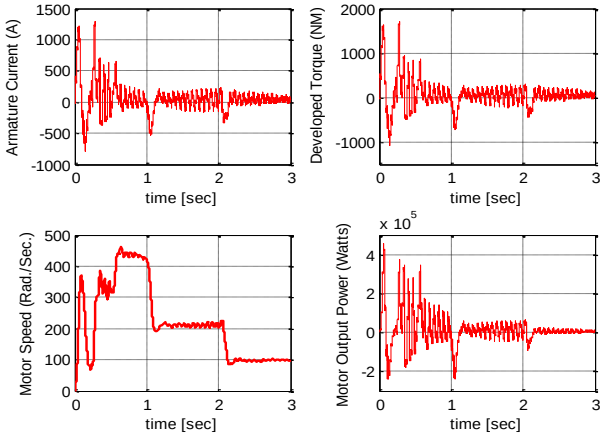

Figure 18 Closed loop characteristics with speed controller + Inner current gain at 0.6 duty cycle.

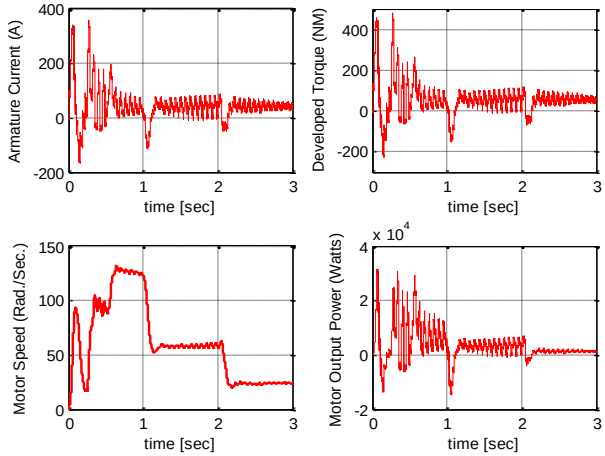

Figure 19 Closed loop characteristics with speed controller + Inner current gain + PI-Controller at 0.6 duty cycle.

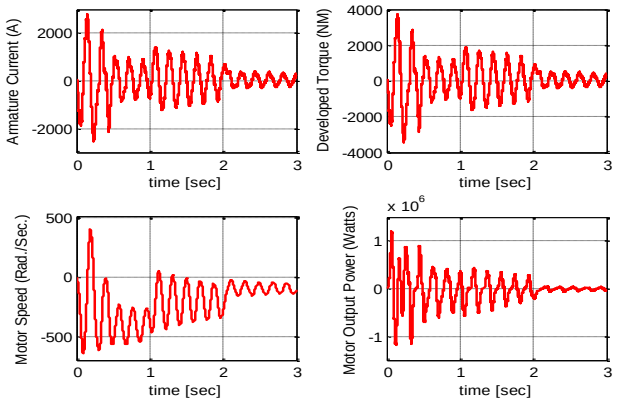

Figure 20 Closed loop characteristics with speed controller at 0.4 duty cycle.

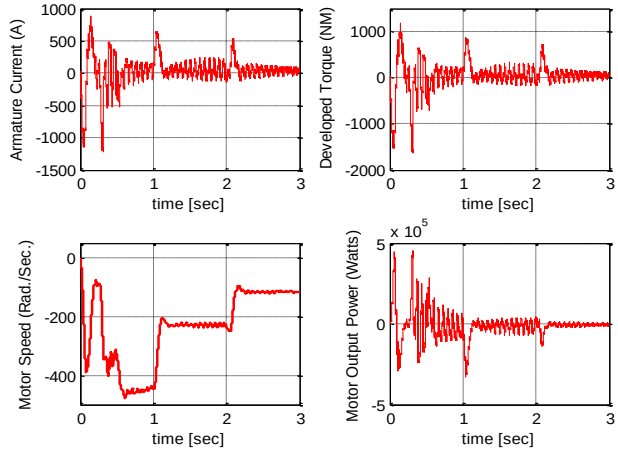

Figure 21 Closed loop characteristics with speed controller + Inner current gain at 0.4 duty cycle.

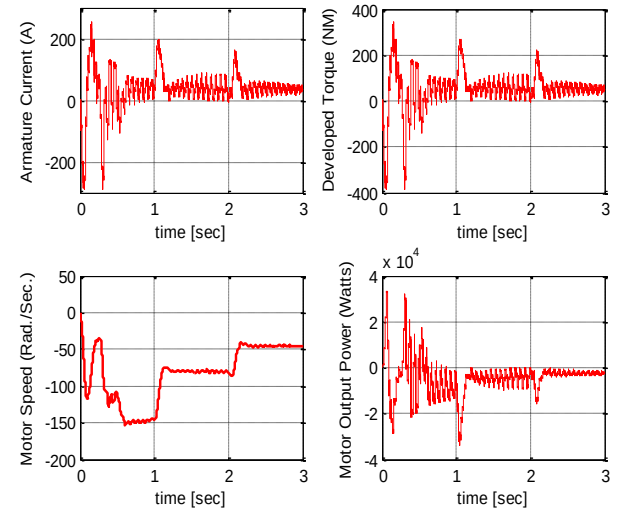

Figure 22 Closed loop characteristics with speed controller + Inner current gain + PI-Controller at 0.4 duty cycle.

5. CONCLUSION

A four quadrant chopper was analyzed at a varied duty cycles of 0.8, 0.6 and 0.4. A separately excited d.c motor was also examined in terms of steady state and dynamic performance characteristics. The steady state performance was analyzed with respect to changes in armature voltage, field flux and varied armature resistance. A sharp decrease in speed-torque characteristic was observed while varying the controlled parameters as reflected in figures 4-7. In the dynamic machine characteristics, three different controlled closed loops were considered at a regulated duty cycles. It is evidently shown in the simulation results presented in figures 14-22 that high starting armature current, developed torque and motor speed are considerably reduced to an acceptable value that corresponds to a reduced duty cycle. The speed regulation values for the three closed loops as presented in table 2 showed a better drive characteristics for closed loop containing speed controller, inner current gain and PI-controller having a higher negative value that conforms to stability analysis.

REFERENCES

B.K Bose "Power Electronics and motor drives recent technology advances" proceedings of the IEEE international symposium on industrial electronics IEEE 2002, pp. 22-25.

S.B Dewan, G.R. Slemmon and A. Straughen. "Power Semi conductor Drives" Wiley Interscience Publisher, 1984.

G.K. Dubey, Fundamentals of Electrical Drives. New Delhi, Narosa publishing House, 2009.

D. Shah, B.T Deshmukh "Reversible D.C Drives Using 4Q IGBT Chopper circuit for industrial Applications" International Journal of Electrical Engineering and Technology Vol.3, issue 1, January 2012, pp. 282-287.

R. Abhinav, J. Masand, P. Vidyarthi, G. Kumari and N. Gupta. "Separately excited d.c motor speed control using four quadrant chopper". International Journal of scientific and Engineering research Vol.4, issue 1, January 2013, pp.1-3.

A. Ansaari, and H. Mehta "Four Quadrant operation of chopper fed separately excited d.c motor by a decoupled PWM control using Digital Signal Processor" International Journal of Science Engineering and Technology Research. Vol.4, issue 5 May 2015, pp. 1720-1729.

O.I. Okoro, C.U. Ogbuka and M.U. Agu "Simulation of DC machine Transient Behaviours: Teachings and Research". The Pacific Journal of Science and Technology, Vol.9, No.1, May 2009, pp.64-78.

G. Jones, G. Joos and T.H. Baton, "Four Quadrant DC Variable Drives, IEEE Proceedings 1975, Vol. 63, No. 12, pp. 1660-1668.

T.H. Abdelhamid, "Performance of single phase DC Drive system controlled by uniform PWM full bridge DC-DC Converter" Electric machines and Drives, 1999. International Conference IEMD' 99. Pp.670-672, May 1999.

M.H. Rashid, Power Electronics Prentice Hall, New Delhi India, 1993.

D.R. Yengalwar, S.S. Zade, D.L. Mute, "Four Quadrant Speed Control of DC Motor Using Chopper" International Journal of Engineering Sciences and Research Technology Vol.4, issue 2, pp.401- 406. Feb. 2015.

P.S. Bimbhra Power Electronics. New Delhi Khanna Publishers, 2006.

N. Mohan T.M. Undeland and W.P. Robbins, Power Electronics Converters, Applications and Design. John Wiley and Sons. New York 2003.

B.K. Bose, Modern Power Electronics and AC Drives Eagle Woods Cliffs, Prentice Hall, PTR Upper Saddle River, 2002.

P.C. Sen and M.L. Mac Donald. Thyristorized D.C Drives with Regenerative Braking and Speed Reversal. IEEE Transactions on Energy Conversion, 1978, Vol. 25, No.4. pp. 347-354.